This is the accepted manuscript made available via CHORUS. The article has been published as:

Directional Limits on Persistent Gravitational Waves from Advanced LIGO's First Observing Run

B. P. Abbott *et al.* (LIGO Scientific Collaboration and Virgo Collaboration)

Phys. Rev. Lett. **118**, 121102 — Published 24 March 2017

DOI: 10.1103/PhysRevLett.118.121102

Directional limits on persistent gravitational waves from Advanced LIGO's first observing run

The LIGO Scientific Collaboration and the Virgo Collaboration*

We employ gravitational-wave radiometry to map the gravitational waves stochastic background expected from a variety of contributing mechanisms and test the assumption of isotropy using data from Advanced LIGO's first observing run. We also search for persistent gravitational waves from point sources with only minimal assumptions over the 20 - 1726 Hz frequency band. Finding no evidence of gravitational waves from either point sources or a stochastic background, we set limits at 90% confidence. For broadband point sources, we report upper limits on the gravitational wave energy flux per unit frequency in the range $F_{\alpha,\Theta}(f) < (0.1 - 56) \times 10^{-8}\,\mathrm{erg\ cm^{-2}\ s^{-1}\ Hz^{-1}}(f/25\ \mathrm{Hz})^{\alpha-1}$ depending on the sky location Θ and the spectral power index α. For extended sources, we report upper limits on the fractional gravitational wave energy density required to close the Universe of $\Omega(f,\Theta) < (0.39-7.6)\times 10^{-8}\,\mathrm{sr}^{-1}(f/25\ \mathrm{Hz})^{\alpha}$ depending on Θ and α. Directed searches for narrowband gravitational waves from astrophysically interesting objects (Scorpius X-1, Supernova 1987 A, and the Galactic Center) yield median frequency-dependent limits on strain amplitude of $h_0 < (6.7,\ 5.5,\ \text{and}\ 7.0) \times 10^{-25}$ respectively, at the most sensitive detector frequencies between 130 – 175 Hz. This represents a mean improvement of a factor of 2 across the band compared to previous searches of this kind for these sky locations, considering the different quantities of strain constrained in each case.

Introduction.—A stochastic gravitational-wave background (SGWB) is expected from a variety of mechanisms [1–5]. Given the recent observations of binary black hole mergers GW150914 and GW151226 [6, 7], we expect the SGWB to be nearly isotropic [8] and dominated [9] by compact binary coalescences [10–12]. The LIGO and Virgo Collaborations have pursued the search for an isotropic stochastic background from LIGO's first observational run [13]. Here, we adopt an eyes-wide-open philosophy and relax the assumption of isotropy in order to allow for the greater range of possible signals. We search for an anisotropic background, which could indicate a richer, more interesting cosmology than current models. We present the results of a generalized search for a stochastic signal with an arbitrary angular distribution mapped over all directions in the sky.

Our search has three components. First, we utilize a broadband radiometer analysis [14, 15], optimized for detecting a small number of resolvable point sources. This method is not applicable to extended sources. Second, we employ a spherical harmonic decomposition [16, 17], which can be employed for point sources but is better suited to extended sources. Last, we carry out a narrowband radiometer search directed at the sky position of three astrophysically interesting objects: Scorpius X-1 (Sco X-1) [18, 19], Supernova 1987 A (SN 1987A) [20, 21], and the Galactic Center (GC) [22].

These three search methods are capable of detecting a wide range of possible signals with only minimal assumptions about the signal morphology. We find no evidence of persistent gravitational waves, and set limits on broadband emission of gravitational waves as a function of sky position. We also set narrowband limits as a function of frequency for the three selected sky positions.

Data.—We analyze data from Advanced LIGO's 4 km detectors in Hanford, WA (H1) and Livingston, LA (L1) during the first observing run (O1), from 15:00 UTC, Sep 18, 2015 – 16:00 UTC, Jan 12, 2016. During O1, the detectors reached an instantaneous strain sensitivity of $7 \times 10^{-24}\,\mathrm{Hz}^{-1/2}$ in the most sensitive region between 100 – 300 Hz , and collected 49.67 days of coincident H1L1 data. The O1 observing run saw the first direct detection of gravitational waves and the first direct observation of merging black holes [6, 7].

For our analysis, the time-series data are downsampled to 4096 Hz from 16 kHz, and divided into 192 s, 50% overlapping, Hann-windowed segments, which are high-pass filtered with a 16th order Butterworth digital filter with knee frequency of 11 Hz (following [13, 23]). We apply data quality cuts in the time domain in order to remove segments associated with instrumental artifacts and hardware injections used for signal validation [24, 25]. We also exclude segments containing known gravitational-wave signals. Finally, we apply a standard non-stationarity cut (see, e.g., [26]), to eliminate segments that do not behave as Gaussian noise. These cuts remove 35% of the data. With all vetoes applied, the total live time for 192 s segments is 29.85 days.

The data segments are Fourier transformed and coarse-grained to produce power spectra with a resolution of 1/32 Hz. This is a finer frequency resolution than the 1/4 Hz used in previous LIGO/Virgo stochastic searches [15, 17] in order to remove many finely spaced instrumental lines occurring at low frequencies. Frequency bins associated with known instrumental artifacts including suspension violin modes [27], calibration lines, electronic lines, correlated combs, and signal injections of

* Full author list given at the end of the article.

persistent, monochromatic, gravitational waves are not included in the analysis. These frequency domain cuts remove 21% of the observing band. For a detailed description of data quality studies performed for this analysis, see the supplement [28] of [13].

The broadband searches include frequencies from 20 – 500 Hz which more than cover the regions of 99% sensitivity for each of the spectral bands (see Table 1 of [13]). The narrowband analysis covers the full 20 – 1726 Hz band.

Method.— The main goal of a stochastic search is to estimate the fractional contribution of the energy density in gravitational waves $\Omega_{\rm gw}$ to the total energy density needed to close the Universe ρ_c. This is defined by

$$\Omega_{\rm gw}(f) = \frac{f}{\rho_c}\frac{d\rho_{\rm gw}}{df} \tag{1}$$

where f is frequency and $d\rho_{\rm gw}$ represents the energy density between f and $f + df$ [29]. For a stationary and unpolarized signal, $\rho_{\rm gw}$ can be factored into an angular power $\mathcal{P}(\Theta)$ and a spectral shape $H(f)$ [30], such that

$$\Omega_{\rm gw}(f) = \frac{2\pi^2}{3H_0^2} f^3 H(f) \int d\Theta\, \mathcal{P}(\Theta), \tag{2}$$

with Hubble constant $H_0 = 68\,{\rm km\,s^{-1}\,Mpc^{-1}}$ from [31].

The angular power $\mathcal{P}(\Theta)$ represents the gravitational wave power at each point in the sky. To express this in terms of the fractional energy density, we define the energy density spectrum as a function of sky position

$$\Omega(f,\Theta) = \frac{2\pi^2}{3H_0^2} f^3 H(f)\mathcal{P}(\Theta). \tag{3}$$

We define a similar quantity for the energy flux, where

$$\mathcal{F}(f,\Theta) = \frac{c^3\pi}{4G} f^2 H(f)\mathcal{P}(\Theta) \tag{4}$$

has units of erg cm^{-2} s^{-1} Hz^{-1} sr^{-1} [15, 16], c is the speed of light and G is Newton's gravitational constant.

Point sources versus extended sources.—We employ two different methods to estimate $\mathcal{P}(\Theta)$ based on the cross-correlation of data streams from a pair of detectors [17, 29]. The radiometer method [14, 15] assumes that the cross-correlation signal is dominated by a small number of resolvable point sources. The point source power is given by $\mathcal{P}_{\Theta_0}$ and the angular power spectrum is then

$$\mathcal{P}(\Theta) \equiv \mathcal{P}_{\Theta_0}\delta^2(\Theta,\Theta_0). \tag{5}$$

Although the radiometer method provides the optimal method for detecting resolvable point sources, it is not well-suited for describing diffuse or extended sources, which may have an arbitrary angular distribution. Hence, we also implement a complementary spherical harmonic decomposition (SHD) algorithm, in which the sky map is decomposed into components $Y_{lm}(\Theta)$ with coefficients $\mathcal{P}_{lm}$ [16]:

$$\mathcal{P}(\Theta) \equiv \sum_{lm} \mathcal{P}_{lm} Y_{lm}(\Theta). \tag{6}$$

Here, the sum over l runs from 0 to $l_{\rm max}$ and $-l \le m \le l$. We discuss the choice of $l_{\rm max}$ below. While the SHD algorithm has comparably worse sensitivity to point sources than the radiometer algorithm, it accounts for the detector response, producing more accurate sky maps.

Spectral models.—In both the radiometer algorithm and the spherical harmonic decomposition algorithm, we must choose a spectral shape $H(f)$. We model the spectral dependence of $\Omega_{\rm gw}(f)$ as a power law:

$$H(f) = \left(\frac{f}{f_{\rm ref}}\right)^{\alpha-3}, \tag{7}$$

where $f_{\rm ref}$ is an arbitrary reference frequency and α is the spectral index (see also [13]). The spectral model will also affect the angular power spectrum, so $\mathcal{P}(\Theta)$ is implicitly a function of α.

We can rewrite the energy density map $\Omega(f,\Theta)$ to emphasize the spectral properties, such that

$$\Omega(f,\Theta) = \Omega_\alpha(\Theta)\left(\frac{f}{f_{\rm ref}}\right)^{\alpha}, \tag{8}$$

where

$$\Omega_\alpha(\Theta) = \frac{2\pi^2}{3H_0^2} f_{\rm ref}^3 \mathcal{P}(\Theta) \tag{9}$$

has units of fractional energy density per steradian $\Omega_{\rm gw}$ sr^{-1}. The spherical harmonic analysis presents skymaps of $\Omega_\alpha(\Theta)$. Note that when $\mathcal{P}(\Theta) = \mathcal{P}_{00}$ (the monopole moment), we recover a measurement for the energy density of the isotropic gravitational wave background. Similarly, the gravitational wave energy flux can be expressed as

$$\mathcal{F}(f,\Theta) = \mathcal{F}_\alpha(\Theta)\left(\frac{f}{f_{\rm ref}}\right)^{\alpha-1}, \tag{10}$$

where

$$\mathcal{F}_\alpha(\Theta) = \frac{c^3\pi}{4G} f_{\rm ref}^2 \mathcal{P}(\Theta). \tag{11}$$

In the radiometer case we calculate the flux in each direction

$$F_{\alpha,\Theta_0} = \frac{c^3\pi}{4G} f_{\rm ref}^2 \mathcal{P}_{\Theta_0}, \tag{12}$$

which is obtained by integrating Equation 11 over the sphere for the point-source signal model described in Equation 5. This quantity has units of erg cm^{-2} s^{-1} Hz^{-1}. Following [13, 32], we choose $f_{\rm ref} =$

25 Hz, corresponding to the most sensitive frequency in the spectral band for a stochastic search with the Advanced LIGO network at design sensitivity.

We consider three spectral indices: $\alpha = 0$, corresponding to a flat energy density spectrum (expected from models of a cosmological background), $\alpha = 2/3$, corresponding to the expected shape from a population of compact binary coalescences, and $\alpha = 3$, corresponding to a flat strain power spectral density spectrum [17, 32]. The different spectral models are summarized in Table I.

Cross Correlation.— A stochastic background would induce low-level correlation between the two LIGO detectors. Although the signal is expected to be buried in the detector noise, the cross-correlation signal-to-noise ratio (SNR) grows with the square root of integration time [29]. The cross correlation between two detectors, with (one-sided strain) power spectral density $P_i(f,t)$ for detector i, is encoded in what is known as "the dirty map" [16]:

$$X_\nu = \sum_{ft} \gamma^*_\nu(f,t) \frac{H(f)}{P_1(f,t)P_2(f,t)} C(f,t). \tag{13}$$

Here, ν is an index, which can refer to either individual points on the sky (the pixel basis) or different lm indices (the spherical harmonic basis). The variable $C(f,t)$ is the cross-power spectral density measured between the two LIGO detectors at some segment time t. The sum runs over all segment times and all frequency bins. The variable $\gamma_\nu(f,t)$ is a generalization of the overlap reduction function, which is a function of the separation and relative orientation between the detectors, and characterizes the frequency response of the detector pair [33]; see [16] for an exact definition.

We can think of X_ν as a sky map representation of the raw cross-correlation measurement before deconvolving the detector response. The associated uncertainty is encoded in the Fisher matrix:

$$\Gamma_{\mu\nu} = \sum_{ft} \gamma^*_\mu(f,t) \frac{H^2(f)}{P_1(f,t)P_2(f,t)} \gamma_\nu(f,t), \tag{14}$$

where * denotes complex conjugation.

Once X_ν and $\Gamma_{\mu\nu}$ are calculated, we have the ingredients to calculate both the radiometer map and the SHD map. However, the inversion of $\Gamma_{\mu\nu}$ is required to calculate the maximum likelihood estimators of GW power $\hat{\mathcal{P}}_\mu = \Gamma^{-1}_{\mu\nu} X_\nu$ [16]. For the radiometer, the correlations between neighbouring pixels can be ignored. The radiometer map is given by

$$\begin{aligned} \hat{\mathcal{P}}_\Theta &= (\Gamma_{\Theta\Theta})^{-1} X_\Theta \\ \sigma^{\rm rad}_\Theta &= (\Gamma_{\Theta\Theta})^{-1/2}, \end{aligned} \tag{15}$$

where the standard deviation $\sigma^{\rm rad}_\Theta$ is the uncertainty associated with the point source amplitude estimator $\hat{\mathcal{P}}_\Theta$, and $\Gamma_{\Theta\Theta}$ is a diagonal entry of the Fisher matrix for a pointlike signal. For the SHD analysis, the full Fisher matrix $\Gamma_{\mu\nu}$ must be taken into account, which includes singular eigenvalues associated with modes to which the detector pair is insensitive. The inversion of $\Gamma_{\mu\nu}$ is simplified by a singular value decomposition regularization. In this decomposition, modes associated with the smallest eigenvalues contribute the least sensitivity to the detector network. Removing a fraction of the lowest eigenmodes "regularizes" $\Gamma_{\mu\nu}$ without significantly affecting the sensitivity (see [16]). The estimator for the SHD and corresponding standard deviation are given by

$$\begin{aligned} \hat{\mathcal{P}}_{lm} &= \sum_{l'm'} (\Gamma^{-1}_R)_{lm,l'm'} X_{l'm'} \\ \sigma^{\rm SHD}_{lm} &= \left[(\Gamma^{-1}_R)_{lm,lm} \right]^{1/2}, \end{aligned} \tag{16}$$

where Γ_R is the *regularized* Fisher matrix. We remove 1/3 of the lowest eigenvalues following [16, 17].

Angular scale.—In order to carry out the calculation in Eq. 16, we must determine a suitable angular scale, which will depend on the angular resolution of the detector network and vary with spectral index α. The diffraction-limited spot size on the sky θ (in radians) is given by

$$\theta = \frac{c}{2df} \approx \frac{50 \text{ Hz}}{f_\alpha}, \tag{17}$$

where $d = 3000$ km is the separation of the LIGO detectors. The frequency f_α corresponds to the most sensitive frequency in the detector band for a power law with spectral index α given the detector noise power spectra [15]. In order to determine f_α we find the frequency at which a power-law with index α is tangent to the single-detector "power-law integrated curve" [34]. The angular resolution scale is set by the maximum spherical harmonic order $l_{\rm max}$, which we can express as a function of α since

$$l_{\rm max} = \frac{\pi}{\theta} \approx \frac{\pi f_\alpha}{50\text{Hz}}. \tag{18}$$

The values of f_α, θ, and $l_{\rm max}$ for three different values of α are shown in Table I. As the spectral index increases, so does f_α, decreasing the angular resolution limit, thus increasing $l_{\rm max}$.

Angular power spectra.—For the SHD map, we calculate the angular power spectra C_l, which describe the angular scale of structure in the clean map, using an unbiased estimator [16, 17]

$$\hat{C}_l \equiv \frac{1}{2l+1} \sum_m \left[|\hat{\mathcal{P}}_{lm}|^2 - (\Gamma^{-1}_R)_{lm,lm} \right]. \tag{19}$$

Narrowband radiometer.—The radiometer algorithm can be applied to the detection of persistent gravitational waves from narrowband point sources associated with a given sky position [15, 17]. We "point" the radiometer in the direction of three interesting sky locations: Sco X-1,

						All-sky (broadband) Results			
						Max SNR (% p-value)		Upper limit range	
α	$\Omega_{\rm gw}$	$H(f)$	f_α (Hz)	θ (deg)	$l_{\rm max}$	BBR	SHD	BBR ($\times 10^{-8}$)	SHD ($\times 10^{-8}$)
0	constant	$\propto f^{-3}$	52.50	55	3	3.32 (7)	2.69 (18)	10 – 56	2.5 – 7.6
2/3	$\propto f^{2/3}$	$\propto f^{-7/3}$	65.75	44	4	3.31 (12)	3.06 (11)	5.1 – 33	2.0 – 5.9
3	$\propto f^{3}$	constant	256.50	11	16	3.43 (47)	3.86 (11)	0.1 – 0.9	0.4 – 2.8

TABLE I. Values of the power-law index α investigated in this analysis, the shape of the energy density and strain power spectrum. The characteristic frequency f_α, angular resolution θ (Eq. 17), and corresponding harmonic order $l_{\rm max}$ (Eq. 18) for each α are also shown. The right hand section of the table shows the maximum SNR, associated significance (p-value) and best upper limit values from the broadband radiometer (BBR) and the spherical harmonic decomposition (SHD). The BBR sets upper limits on energy flux [erg cm^{-2} s^{-1} Hz$^{-1}(f/25$ Hz$)^{\alpha-1}$] while the SHD sets upper limits on the normalized energy density [sr$^{-1}(f/25$ Hz$)^{\alpha}$] of the SGWB.

the Galactic Center, and the remnant of supernova SN 1987A.

Scorpius X-1 (Sco X-1) is a low-mass X-ray binary believed to host a neutron star that is potentially spun up through accretion, in which gravitational wave emission may provide a balancing spin-down torque [18, 19, 35, 36]. The frequency of the gravitational wave signal is expected to spread due to the orbital motion of the neutron star. At frequencies below ∼930 Hz this Doppler line broadening effect is less than 1/4 Hz, the frequency bin width selected in past analyses [15, 17]. At higher frequencies, the signal is certain to span multiple bins. We therefore combine multiple 1/32 Hz frequency bins to form optimally sized *combined bins* at each frequency, accounting for the expected signal broadening due to the combination of the motion of the Earth around the Sun, the binary orbital motion, and any other intrinsic modulation. For more detail on the method of combining bins, see the technical supplement to this paper [37].

The possibility of a young neutron star in SN 1987A [20, 21] and the likelihood of many unknown, isolated neutron stars in the Galactic Center region [22] indicate potentially interesting candidates for persistent gravitational wave emission. We combine bins to include the signal spread due to Earth's modulation. For SN 1987A, we choose a combined bin size of 0.09 Hz. We would be sensitive to spin modulations up to $|\dot{\nu}| < 9\times10^{-9}$ Hz s^{-1} within our O1 observation time spanning 116 days. The Galactic Center is at a lower declination with respect to the orbital plane of the Earth. The Earth modulation term is therefore more significant so for the Galactic Center we choose combined bins of 0.53 Hz across the band. In this case we are sensitive to a frequency modulation in the range $|\dot{\nu}| < 5.3\times10^{-8}$ Hz s^{-1}.

Significance.—To assess the significance of the SNR in the combined bins of the narrowband radiometer spectra, we simulate many realizations of the strain power consistent with Gaussian noise in each individual frequency bin. Combining these in the same way as the actual analysis leaves us with a distribution of maximum SNR values across the whole frequency band for many simulations of noise.

For a map of the whole sky, the distribution of maximum SNR is complicated by the many dependent trials due to covariances between different pixels (or patches) on the sky. We calculate this distribution numerically by simulating many realizations of the dirty map X_ν with expected covariances described by the Fisher matrix $\Gamma_{\mu\nu}$ (cf. Eqs. 13 and 14, respectively). This distribution is then used to calculate the significance (or p-value) of a given SNR recovered from the sky maps [17]. We take a p-value of 0.01 or less to indicate a significant result. The absence of any significant events indicates the data are consistent with no signal being detected, in which case we quote Bayesian upper limits at 90% confidence [15, 17]

Results—The search yields four data products:

Radiometer sky maps, optimized for broadband point sources, are shown in Fig. 1. The top row shows the SNR. Each column corresponds to a different spectral index, $\alpha = 0$, 2/3 and 3, from left to right, respectively. The maximum SNRs are respectively 3.32, 3.31, and 3.43 corresponding to false-alarm probabilities typical of what would be expected from Gaussian noise; see Table I. We find no evidence of a signal, and so set limits on gravitational-wave energy flux, which are provided in the bottom row of Fig. 1 and summarized in Table I.

SHD sky maps, suitable for characterizing an anisotropic stochastic background, are shown in Fig. 2. The top row shows the SNR and each column corresponds to a different spectral index ($\alpha = 0$, 2/3 and 3, respectively). The maximum SNRs are 2.96, 3.06, and 3.86 corresponding to false-alarm probabilities typical of those expected from Gaussian noise; see Table I. Failing evidence of a signal, we set limits on energy density per unit solid angle, which are provided in the bottom row of Fig. 2 and summarised in Table I. Interactive visualizations of the SNR and upper limit maps are also available online [38].

Angular power spectra are derived from the SHD sky maps. We present upper limits at 90% confidence on the angular power spectrum indices C_l from the spherical harmonic analysis in Figure 3.

Radiometer spectra, suitable for the detection of

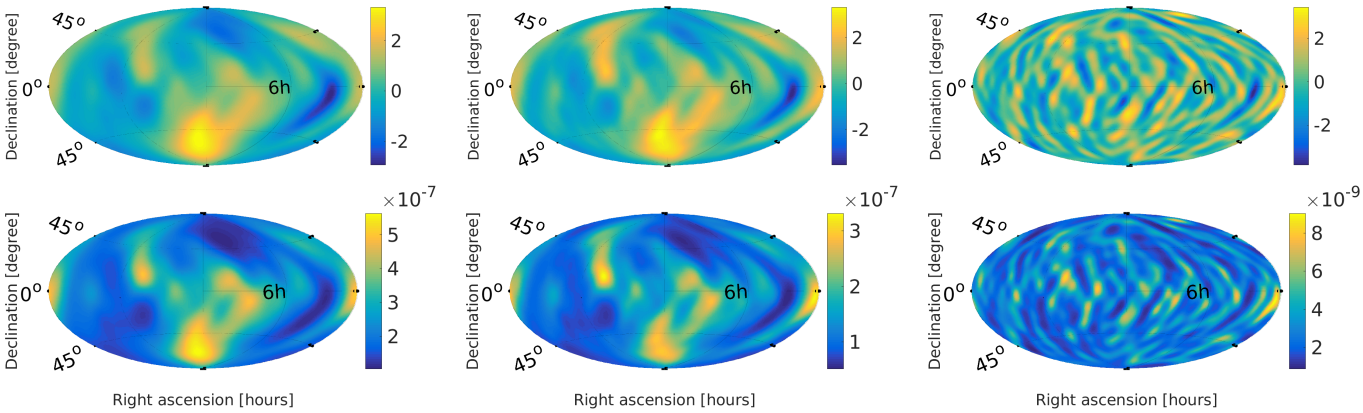

FIG. 1. All-sky radiometer maps for point-like sources showing SNR (top) and upper limits at 90% confidence on energy flux F_{α,Θ_0} [erg cm^{-2} s^{-1} Hz^{-1}] (bottom) for three different power-law indices, $\alpha = 0$, 2/3 and 3, from left to right, respectively. The p-values associated with the maximum SNR are (from left to right) $p = 7\%$, $p = 12\%$, $p = 47\%$ (see Table I).

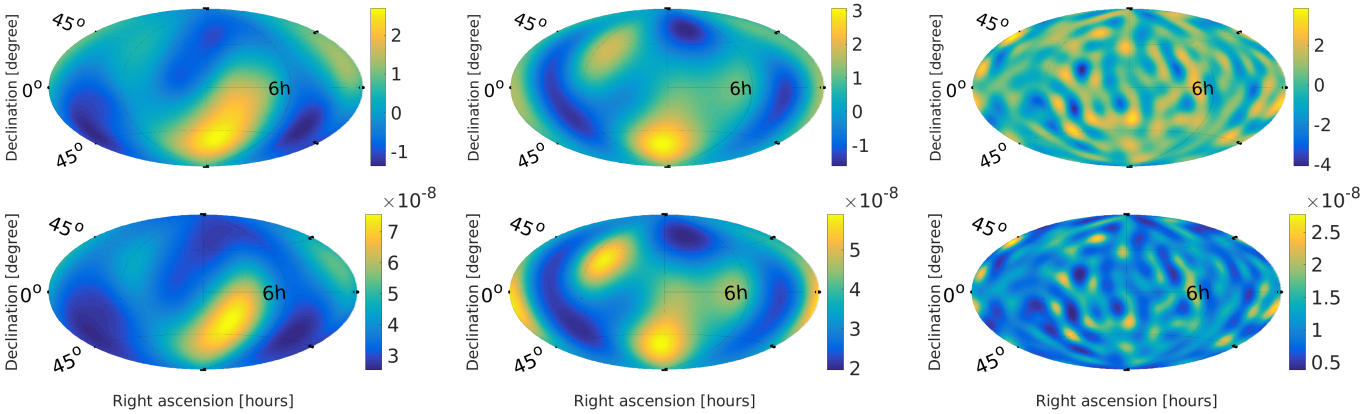

FIG. 2. All-sky spherical harmonic decomposition maps for extended sources showing SNR (top) and upper limits at 90 % confidence on the energy density of the gravitational wave background Ω_α [sr^{-1}] (bottom) for three different power-law indices $\alpha = 0$, 2/3 and 3, from left to right, respectively. The p-values associated with the maximum SNR are (from left to right) $p = 18\%$, $p = 11\%$, $p = 11\%$ (see Table I).

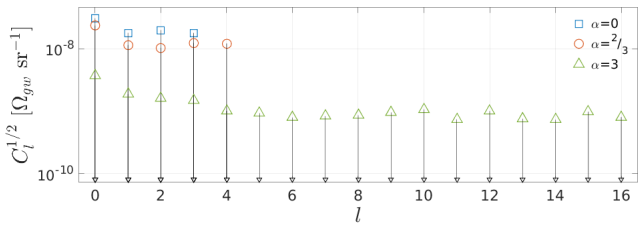

FIG. 3. Upper limits on C_l at 90% confidence vs l for the SHD analyses for $\alpha = 0$ (top, blue squares), $\alpha = 2/3$ (middle, red circles) and $\alpha = 3$ (bottom, green triangles).

a narrowband point source associated with a given sky position, are given in Fig. 4, the main results of which are summarised in Table II. For the three sky locations (Sco X-1, SN 1987A and the Galactic Center), we calculate the SNR in appropriately sized combined bins across the LIGO band. For Sco X-1, the loudest observed SNR is 4.58, which is consistent with Gaussian noise. For SN 1987A and the Galactic Center, we observe maximum SNRs of 4.07 and 3.92 respectively, corresponding to false alarm probabilities consistent with noise; see Table II.

Since we observe no statistically significant signal, we set 90% confidence limits on the peak strain amplitude h_0 for each optimally sized frequency bin. Upper limits were set using a Bayesian methodology with the constraint that $h_0 > 0$ and validated with software injection studies. The upper limit procedure is described in more detail in the technical supplement [37], while the subsequent software injection validation is detailed in [39].

The results of the narrowband radiometer search for the three sky locations are shown in Fig. 4. To avoid setting limits associated with downward noise fluctuations, we take the median upper limit from the most sensitive 1 Hz band as our best strain upper limit. We obtain 90% confidence upper limits on the gravitational wave strain of $h_0 < 6.7 \times 10^{-25}$ at 134 Hz , $h_0 < 7.0 \times 10^{-25}$ at 172 Hz and $h_0 < 5.5 \times 10^{-25}$ at 172 Hz from Sco X-1, SN 1987A and the Galactic Center respectively in

Narrowband Radiometer Results

Direction	Max SNR	p-value (%)	Frequency band (Hz)	Best UL ($\times 10^{-25}$)	Frequency band (Hz)
Sco X-1	4.58	10	$616 - 617$	6.7	$134 - 135$
SN1987A	4.07	63	$195 - 196$	5.5	$172 - 173$
Galactic Center	3.92	87	$1347 - 1348$	7.0	$172 - 173$

TABLE II. Results for the narrowband radiometer showing the maximum SNR, corresponding p-value and 1 Hz frequency band as well as the 90% gravitational wave strain upper limits, and corresponding frequency band, for three sky locations of interest. The best upper limits are taken as the median of the most sensitive 1 Hz band.

the most sensitive part of the LIGO band

Conclusions. We find no evidence to support the detection of either point-like or extended sources and set upper limits on the energy flux and energy density of the anisotropic gravitational wave sky. We assume three different power law models for the gravitational wave background spectrum. Our mean upper limits present an improvement over initial LIGO results of a factor of 8 in flux for the $\alpha = 3$ broadband radiometer and factors of 60 and 4 for the spherical harmonic decomposition method for $\alpha = 0$ and 3 respectively [17, 40]. We present the first upper limits for an anisotropic stochastic background dominated by compact binary inspirals (with an $\Omega_{\rm gw} \propto f^{2/3}$ spectrum) of $\Omega_{2/3}(\Theta) < 2 - 6 \times 10^{-8}$ sr^{-1} depending on sky position. We can directly compare the monopole moment of the spherical harmonic decomposition to the isotropic search point estimate $\Omega_{2/3} = (3.5 \pm 4.4) \times 10^{-8}$ from [13]. We obtain $\Omega_{2/3} = (2\pi^2/3H_0^2) f_{\rm ref}^3 \sqrt{4\pi}\mathcal{P}_{00} = (4.4 \pm 6.4) \times 10^{-8}$. The two results are statistically consistent. Our spherical harmonic estimate of $\Omega_{2/3}$ has a larger uncertainty than the dedicated isotropic search because of the larger number of (covariant) parameters estimated when $l_{\rm max} > 0$. We also set upper limits on the gravitational wave strain from point sources located in the directions of Sco X-1, the Galactic Center and Supernova 1987A. The narrowband results improve on previous limits of the same kind by more than a factor of 10 in strain at frequencies below 50 Hz and above 300 Hz, with a mean improvement of a factor of 2 across the band [17].

Acknowledgments.—The authors gratefully acknowledge the support of the United States National Science Foundation (NSF) for the construction and operation of the LIGO Laboratory and Advanced LIGO as well as the Science and Technology Facilities Council (STFC) of the United Kingdom, the Max-Planck-Society (MPS), and the State of Niedersachsen/Germany for support of the construction of Advanced LIGO and construction and operation of the GEO600 detector. Additional support for Advanced LIGO was provided by the Australian Research Council. The authors gratefully acknowledge the Italian Istituto Nazionale di Fisica Nucleare (INFN), the French Centre National de la Recherche Scientifique (CNRS) and the Foundation for Fundamental Research on Matter supported by the Netherlands Organisation for Scientific Research, for the construction and operation of the Virgo detector and the creation and support of the EGO consortium. The authors also gratefully acknowledge research support from these agencies as well as by the Council of Scientific and Industrial Research of India, Department of Science and Technology, India, Science & Engineering Research Board (SERB), India, Ministry of Human Resource Development, India, the Spanish Ministerio de Economía y Competitividad, the Conselleria d'Economia i Competitivitat and Conselleria d'Educació, Cultura i Universitats of the Govern de les Illes Balears, the National Science Centre of Poland, the European Commission, the Royal Society, the Scottish Funding Council, the Scottish Universities Physics Alliance, the Hungarian Scientific Research Fund (OTKA), the Lyon Institute of Origins (LIO), the National Research Foundation of Korea, Industry Canada and the Province of Ontario through the Ministry of Economic Development and Innovation, the Natural Science and Engineering Research Council Canada, Canadian Institute for Advanced Research, the Brazilian Ministry of Science, Technology, and Innovation, Fundação de Amparo à Pesquisa do Estado de São Paulo (FAPESP), Russian Foundation for Basic Research, the Leverhulme Trust, the Research Corporation, Ministry of Science and Technology (MOST), Taiwan and the Kavli Foundation. The authors gratefully acknowledge the support of the NSF, STFC, MPS, INFN, CNRS and the State of Niedersachsen/Germany for provision of computational resources. This is LIGO document LIGO-P1600259.

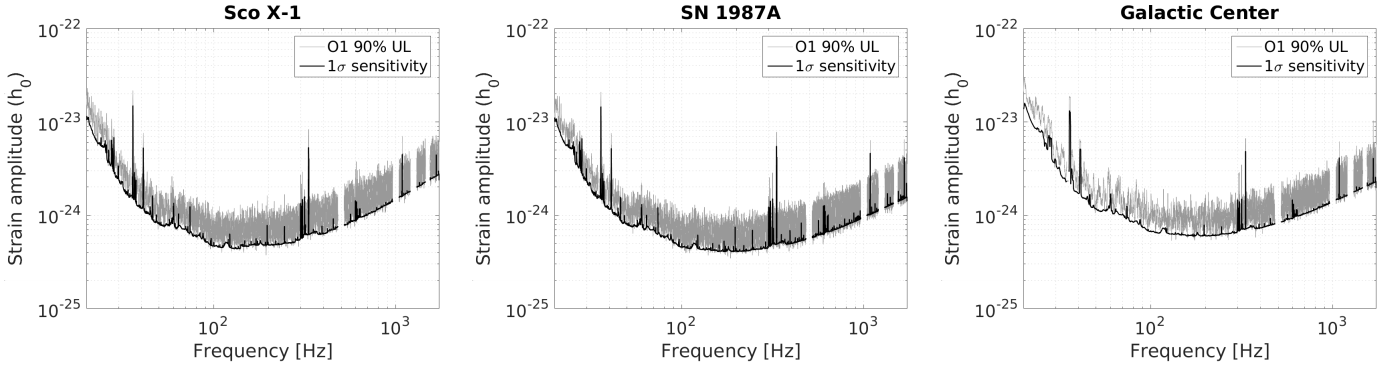

FIG. 4. Radiometer 90% upper limits on dimensionless strain amplitude (h_0) as a function of frequency for Sco X-1 (left), SN1987A (middle) and the Galactic Center (right) for the O1 observing run (gray band) and standard deviation σ (black line). The large spikes correspond to harmonics of the 60 Hz power mains, calibration lines and suspension-wire resonances.

[1] M. Maggiore, Phys. Rep. **331**, 283 (2000).
[2] B. Allen, in *Relativistic Gravitation and Gravitational Radiation*, edited by J.-A. Marck and J.-P. Lasota (1997) p. 373, gr-qc/9604033.
[3] V. Mandic and A. Buonanno, Phys. Rev. D **73**, 063008 (2006).
[4] X.-J. Zhu, X.-L. Fan, and Z.-H. Zhu, Astrophys. J. **729**, 59 (2011).
[5] X. Siemens, V. Mandic, and J. Creighton, Phys. Rev. Lett. **98**, 111101 (2007).
[6] B. P. Abbott *et al.* (LIGO Scientific Collaboration and Virgo Collaboration), Phys. Rev. Lett.. **116**, 061102 (2016).
[7] B. P. Abbott and others. (LIGO Scientific Collaboration and Virgo Collaboration), Phys. Rev. Lett. **116**, 241103 (2016).
[8] D. Meacher, E. Thrane, and T. Regimbau, Phys. Rev. D **89**, 084063 (2014).
[9] T. Callister, L. Sammut, S. Qiu, I. Mandel, and E. Thrane, Phys. Rev. X **6**, 031018 (2016).
[10] T. Regimbau and B. Chauvineau, Class. Quantum Gravity **24**, S627 (2007).
[11] C. Wu, V. Mandic, and T. Regimbau, Phys. Rev. D **85**, 104024 (2012).
[12] X.-J. Zhu, E. J. Howell, D. G. Blair, and Z.-H. Zhu, Mon. Not. R. Astron Soc. **431**, 882 (2013).
[13] The LIGO Scientific Collaboration and the Virgo Collaboration, ArXiv e-prints (2016), arXiv:1612.02029 [gr-qc].
[14] S. W. Ballmer, Class. Quantum Gravity **23**, S179 (2006).
[15] B. Abbott *et al.*, Phys. Rev. D **76**, 082003 (2007).
[16] E. Thrane, S. Ballmer, J. D. Romano, S. Mitra, D. Talukder, S. Bose, and V. Mandic, Phys. Rev. D **80**, 122002 (2009).
[17] J. Abadie *et al.*, Phys. Rev. Lett. **107**, 271102 (2011).
[18] J. Aasi *et al.*, Phys. Rev. D **91**, 062008 (2015).
[19] C. Messenger *et al.*, Phys. Rev. D **92**, 023006 (2015).
[20] C. T. Y. Chung, A. Melatos, B. Krishnan, and J. T. Whelan, Mon. Not. R. Astron Soc. **414**, 2650 (2011).
[21] L. Sun, A. Melatos, P. D. Lasky, C. T. Y. Chung, and N. S. Darman, Phys. Rev. D **94**, 082004 (2016).
[22] J. Aasi *et al.*, Phys. Rev. D **88**, 102002 (2013).
[23] B. Abbott *et al.*, Astrophys. J. **659**, 918 (2007).
[24] B. P. Abbott *et al.*, Class. Quantum Gravity **33**, 134001 (2016).
[25] C. Biwer *et al.*, ArXiv e-prints (2016), arXiv:1612.07864 [astro-ph.IM].
[26] B. P. Abbott *et al.*, Nature **460**, 990 (2009).
[27] S. M. Aston *et al.*, Classical and Quantum Gravity **29**, 235004 (2012).
[28] See Supplemental Material of [13] at [URL will be inserted by publisher] for more detail on the data quality studies performed during this analysis.
[29] B. Allen and J. D. Romano, Phys. Rev. D **59**, 102001 (1999).
[30] B. Allen and A. C. Ottewill, Phys. Rev. D **56**, 545 (1997).
[31] Planck Collaboration, P. A. R. Ade, *et al.*, Astron. Astrophys. **571**, A1 (2014).
[32] B. P. Abbott *et al.*, Phys. Rev. Lett. **116**, 131102 (2016).
[33] N. Christensen, Phys. Rev. D **46**, 5250 (1992).
[34] E. Thrane and J. D. Romano, Phys. Rev. D **88**, 124032 (2013).
[35] L. Bildsten, Astrophys. J. Lett. **501**, L89 (1998).
[36] B. Abbott *et al.*, Phys. Rev. D **76**, 082001 (2007).
[37] See Supplemental Material of this article at [URL will be inserted by publisher] for details on the directed narrowband radiometer procedure to calcuate upper limits on the gravitational wave strain amplitude.
[38] B. P. Abbott *et al.* (LIGO Scientific Collaboration and Virgo Collaboration), "Mapping a stochastic gravitational wave background," (2016), `https://dcc.ligo.org/public/0139/G1602343/002/index.html`.
[39] B. P. Abbott *et al.* (LIGO Scientific Collaboration and Virgo Collaboration), "O1 stochastic narrowband radiometer injection recovery summary," (2016), `https://dcc.ligo.org/LIGO-T1600563`.
[40] The spherical harmonic analysis uses different values of the maximum order $l_{\max}$ than those used in [17]. The $l_{\max}$ value was decreased by a factor of 2 for $\alpha = 0$ and increased by 30% for $\alpha = 3$. The harmonic order resembles extra degrees of freedom, meaning that larger values of $l_{\max}$ tend to reduce the sensitivity in $\Omega_{\rm gw}$ by increasing uncertainty in estimates of the angular power $\mathcal{P}(\Theta)$.